

Tunable-focus liquid lens actuated by a novel piezoelectric motor

Hanlu Li¹ , Weihao Ren¹ , Lin Yang¹ , Chengcheng Ma²,
Siyu Tang³ and Ruijia Yuan¹

Proc IMechE Part C:
J Mechanical Engineering Science
0(0) 1–11
© IMechE 2020
Article reuse guidelines:
sagepub.com/journals-permissions
DOI: 10.1177/0954406220971666
journals.sagepub.com/home/pic



Abstract

In this paper, a tunable-focus liquid lens driven by a novel piezoelectric motor is proposed for the adaptive application. Compressing the liquid chamber, the curvature of the lens can be changed by increasing the liquid pressure. This mechanism requires the motor to provide a vertical force to deform the lens surface, whose curvature can be decreased and thereby increasing its focus. As a key part of the tunable-focus liquid lens, a novel piezoelectric motor with the compact structure is emphatically developed in this paper. The operation process of the motor is discussed in detail, whose geometrical parameters are calculated by the finite element simulations. And the motor prototype is then fabricated and tested by the experimental platform. The testing results indicate that the motor can operate steadily and continuously, whose maximum linear velocity can reach 0.065 mm/s under the frequency of 11.80 kHz and voltage of 400 V_{p-p}. The measurement shows that the proposed lens driven by the piezoelectric motor can zoom ranged from 9.6 mm to 17.9 mm, which is suitable for adaptive eyeglass application. Compared with other liquid lens, the prototype with a compact structure, easy and low cost fabrication process can provide high-precision adjustment within a certain range. The presented device exhibits well zooming characteristic and stability in the experiment, which also realizes the successful application of piezoelectric motor in the liquid-lens. It shows greatly potential in the adaptive eyeglasses, and may be employed as the mobile system in the near future.

Keywords

Piezoelectric motor, tunable-focus, liquid lens, membrane, focal length

Date received: 24 June 2020; accepted: 14 October 2020

Introduction

For decades, visual impairment has been grown into a considerable public health issue all over the world. By the end of 2019, about 1.91 billion people had suffered from severe visual impairments.^{1,2} In particular, the presbyopia, regarded as an age-related vision problem,³ has received extensive attention worldwide. Some researches indicate that the thickness of our cornea will increase after the age of 45, obviously over 65.^{4–6} Such impairment is a phenomenon of the classical refractive error, which is unavoidable but can be corrected by the corrective lenses.^{7,8} However, the eyeglasses currently used in the treatment of the presbyopia have a fixed refraction, which cannot correct the refractive errors of eyes in time under variable applications.^{9,10} Therefore, it is necessary to develop a tunable-focus lens to correct refractive errors of the presbyopia.

The adaptive liquid lens is an intelligent optical system, which has been realized by several different mechanisms to change the lens optical power.^{11–13}

According to the principle of the adaptive lens, it can be classified into three categories. The first type is the lens via the mechanical transmission. Peter Liebetraut¹⁴ put forward a new-type elastomeric lens with tunable astigmatism. In the lens, four servo motors were used to generate the asymmetric deformation of the membrane. The adjustment of the focal length could be achieved by controlling strain, but its control scheme was relatively complicated. Secondly, the refracting power of the lens can also be controlled by the hydraulic system. Ki-Hun

¹State Key Laboratory of Mechanics and Control of Mechanical Structures, Nanjing University of Aeronautics and Astronautics, Nanjing, China

²Shanghai Aerospace Control Technology Institute, Shanghai, China

³Nuaa Super Control Technology Co., Ltd, Nanjing, China

Corresponding author:

Lin Yang, State Key Laboratory of Mechanics and Control of Mechanical Structures, Nanjing University of Aeronautics and Astronautics, Nanjing 210016, China.

Email: yanglin@nuaa.edu.cn

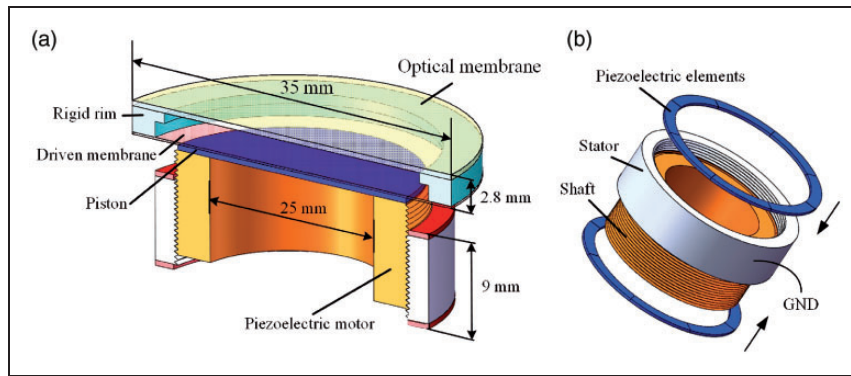


Figure 1. Configuration of the liquid lens: (a) Structure diagram of the proposed lens. (b) Configuration of the proposed piezoelectric motor.

Jeong¹⁵ proposed a tunable micro-doublet lens driven by the hydraulic system. Meanwhile, H.Oku from Japan¹⁶ stated that the shape of the lens could be controlled by pumping liquid in or out, which was quite sensitive to the gravity and temperature. As for the third one, the focal length was accommodated by the deformation of the intelligent materials. In 2015, Stephane Nicolas¹⁷ presented a compact liquid lens with an embedded piezoelectric actuator, which has excellent optical performances. This kind of lens had the advantages of the compact structure and easy processing, but its zoom range is greatly limited. In addition, for the piezoelectric actuators^{18–20} are characterized by hysteresis behaviour, it is difficult to locate the desired focal length precisely.

In conclusion, several approaches of the liquid lens with different structures have been reported. However, many of them cannot enlarge the range of the tunable focal length while ensuring lens's response speed. This defect limits the development of the variable-focus lens greatly.²¹ Therefore, it is essential to design a tunable-focus liquid lens with novel focusing mechanism.

Unlike traditional motors, piezoelectric motor is a new-type actuator based on the converse piezoelectric effect.²² It has many advantages such as quickly response, off power self-locking and anti-electromagnetic interference. For its excellent mechanical properties, it is widely used in micro-devices, especially the focusing system of the camera.^{23–25} The research of piezoelectric motors may provide a new idea for developing the novel liquid lens.

In order to solve the problems existed in the liquid lens, a tunable-focus lens driven by a novel piezoelectric motor with aperture diameter of 30 mm is proposed, assembled and investigated in this paper. By actuating the piezoelectric motor, the shape of the lens surface can be changed, which are calculated using the finite element method in the software of Ansys 18.0. To achieve the feasibility of the tunable-focus lens, the proposed linear piezoelectric motor is used as the actuator to deform the lens surface.

The motor's operating principle is demonstrated in detail, whose modal analysis and dynamic response analysis is accomplished by simulating calculation. The prototype lens is eventually fabricated, whose performances are tested by the experimental platform.

Structure and operating principle

Configuration of the liquid lens

This paper introduces a novel varifocal lens actuated by the piezoelectric motor, whose configuration is shown in the Figure 1(a). The key features of the lens are its compact structure and simple operation. The chamber of the lens is encapsulated by a rigid rim and flexible membranes, which is used to store the transparent liquid of high-index. The top membrane is called the optical membrane, whose deformation reflects the lens's optical performances directly. And the bottom membrane is regarded as the driven membrane, which can bear external load transmitted by the piston.

A novel piezoelectric motor placed under the piston, is composed of a stator, an output shaft and piezoelectric elements, as shown in the Figure 1(b). The stator is a cylinder with fine threads on its inner surface, and the piezoelectric elements are bonded on the end faces of the cylinder correspondingly. Under the excitation of the voltage, the travelling wave can be excited in the stator by utilizing the converse piezoelectric effect of the elements. The vibration on the stator's surface of will drive the shaft to rotate through applying a certain pre-pressure. And the rotation motion will be transformed into a linear motion by threads, which can provide a driving force along the axial direction for the lens.

When an axial force is applied to the piston, the shape of the driven membrane will deform. The pressure endured on the membrane therefore is improved and transmitted to the liquid. By this stage, the sealed space is compressed, the liquid stored in this space

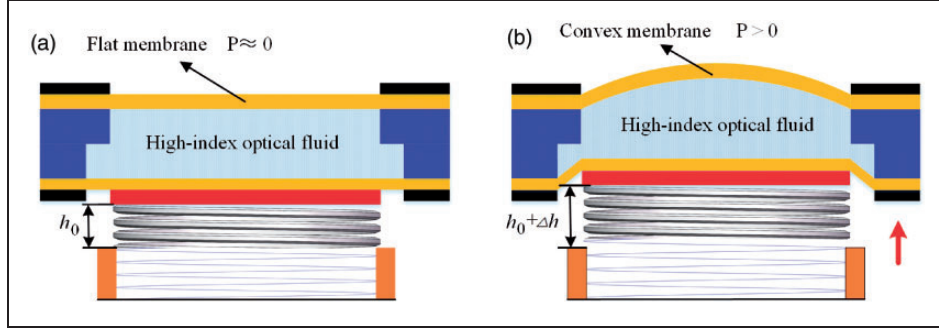


Figure 2. Working principle of the tunable-focus liquid lens: (a) No focus effect with shaft's linear displacement of 0. (b) Focus effect with shaft's linear displacement of Δh .

will be redistributed, thereby deforming the optical membrane. The shape of the optical membrane can be adjusted by controlling the rise displacement of the shaft, whose working principle is illustrated in the Figure 2. Thus, the convex lenses with required focus can be realized by controlling the motor easily. The proposed lens not only provides a new driving method for the liquid lens, but also broadens the further application of piezoelectric motor in the focus systems.

Operating principle

To generate a travelling wave in the stator, two orthogonal modes with the same order are required to excite by combining the piezoelectric ceramics properly.²⁶ According to this principle, a piezoelectric ring is divided into 8 parts uniformly and polarized along its thickness direction, as depicted in the Figure 3(a). These partitions are divided into Group A and Group B, on which alternating signals are the voltages with a phase difference of $\pi/2$. Under the voltage excitation, two orthogonal bending modes are excited in the stator. Figure 3(b) and (c) describe the shape of excited modes in the geometric neutral layer of the stator. Theoretically, these two bending modes have the same shape, and their phase difference is $\pi/2$. By superposing the operating modes, the travelling wave can be obtained in the stator, thus the point on the driving surface moves in an ellipse.

For explaining the motor's driving mechanism more clearly, the spread procedure of the travelling wave is demonstrated in the Figure 4. An arbitrary point P shown in the Figure 4(a) is selected as the particle to be analyzed, whose trajectory is a counter-clockwise ellipse. To acquire the vibration of P along radial and circumferential direction, the stator is expanded in the plane XOY displayed in the Figure 4(b). With the advances of the travelling wave, Particle P experiences the transformation of (1)→(2)→(3)→(4)→(1), as shown in the Figure 4(b). This action enables the particle to move along the elliptic orbit in a single period, which pushes the shaft to rotate and convert into the linear movement along

the axial direction. As for the direction of the linear movement, it can be reversed by adjusting the phases of exciting voltages.

Numerical simulation

Analysis of the lens surface

The optical membrane, as the elastic surface of the lens, plays an important role in the design of the lens's configuration. Thus, it is necessary to analysis the surface deformation, which provides a solid basis for the further study. Considering the unique properties of the liquid lens, the selected membrane should have the excellent optical characteristics and better elasticity. Polydimethylsiloxane (PDMS) is a silicone rubber with excellent stability physically and chemically, which can generate relatively large deformation without damaging its structure. For its prominent mechanical performances, the material has been used widely in the microfluidic devices.²⁷

According to the principle of energy conversation, the strain energy potential of PDMS can be described as,²⁸

$$W = C_{10} \cdot (\bar{I}_1 - 3) + C_{01} \cdot (\bar{I}_2 - 3) + \frac{1}{d} \cdot (J - 1) \quad (1)$$

Where \bar{I}_1 and \bar{I}_2 represent the first and second strain invariant respectively. J is a determinant of the elastic deformation gradient. In addition, C_{10} and C_{01} are the constants characterizing the deviatoric deformation of the material.

Moreover, d is a parameter to describe the incompressibility of the material, which can be written as,

$$d = \frac{6 \cdot (1 - 2\nu)}{E} \quad (2)$$

Where E and ν are the Young's modulus and Poisson's ratio of the material respectively, which can be adjusted by changing the ratio of the polymer

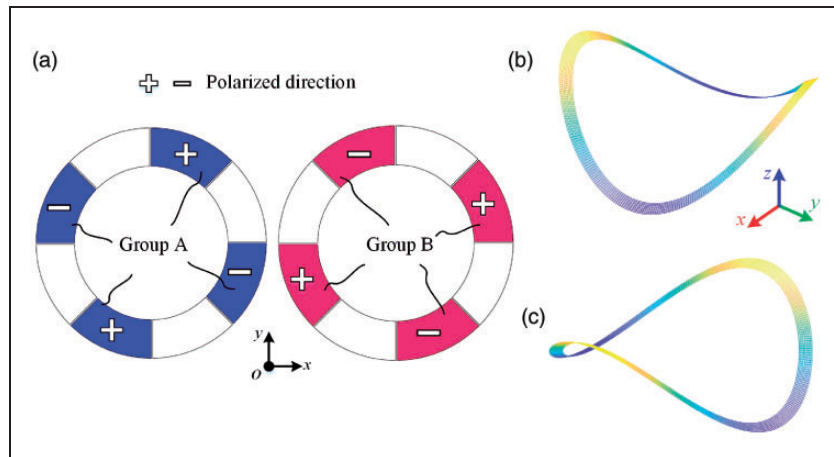


Figure 3. Modes of the proposed piezoelectric motor: (a) Polarization of the piezoelectric ceramics. (b) Excited mode A of the stator's geometric neutral layer. (c) Excited mode B of the stator's geometric neutral layer.

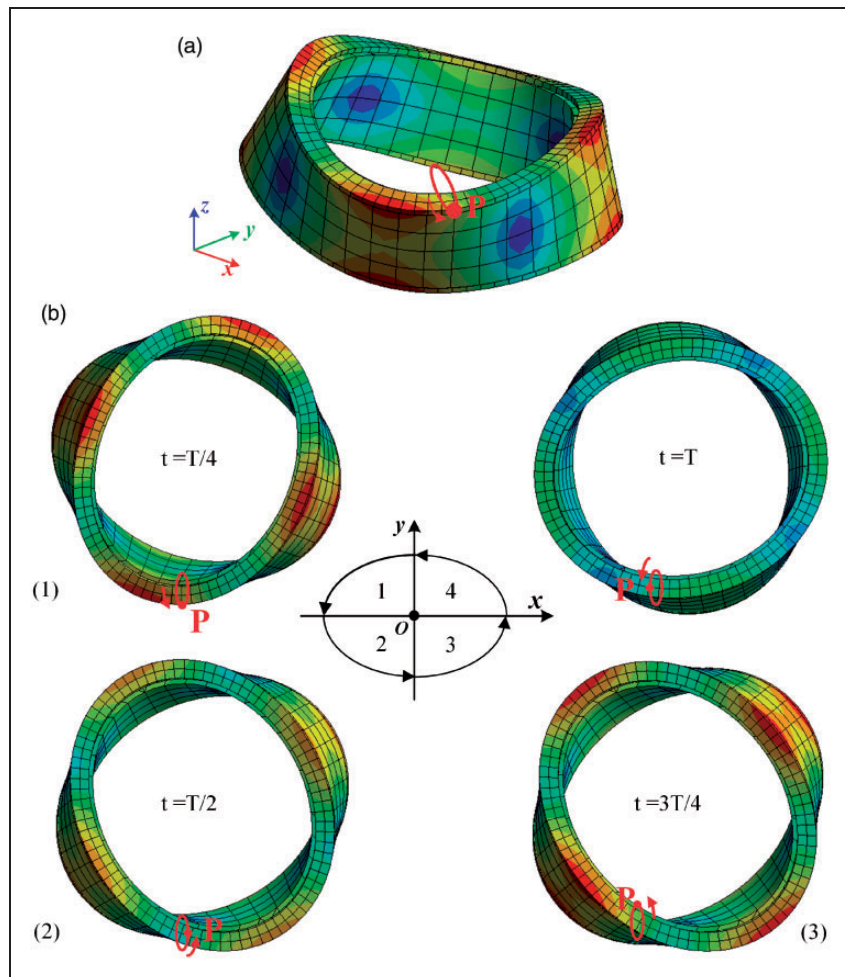


Figure 4. Driving mechanism of the proposed motor: (a) Selected point on the surface of the stator. (b) Schematic diagram of its working principle.

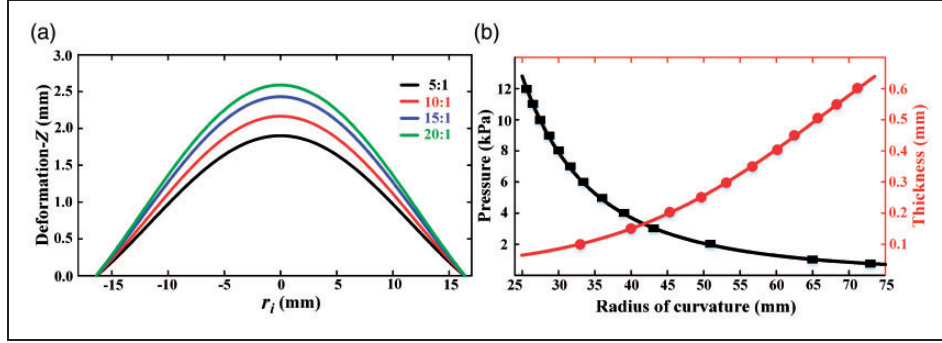
to the curing agent. Table 1 shows the material parameters at four different mixing ratios.

For the material has the nonlinearity geometricaly, the analysis of the membrane's deformation is completed by ANSYS. In the simulation, the

membrane is simplified as a shell unit with radius 33 mm and thickness 0.5 mm. When the periphery is fixed completely, the deformed surface is alike a paraboloid. Figure 5(a) shows the deformation of the membrane at four different mixing ratios.

Table 1. Material parameters of PDMS under various mixing ratio.

Mixing ratio	Young's modulus (MPa)	Poisson's ratio	C_{10}	C_{01}	d
5:1	4.1458	0.47	0.564054422	0.141013605	0.085098172
10:1	2.9733	0.475	0.403159322	0.100789831	0.099216359
15:1	2.1704	0.48	0.293297297	0.073324324	0.109104313
20:1	1.8145	0.48	0.245202703	0.061300676	0.130504271

**Figure 5.** Simulation results of the lens surface: (a) Deformation of the elastic surface under different mixing ratios of PDMS. (b) Relationship of membrane's radius of curvature with different pressures and thickness.

It can be seen from the image that the deflection reaches peak at its rotational center, and the maximum value can be varied by increasing the mixing ratio of the material.

Furthermore, if the standard spherical profile with the same deflection is adopted to analyze the elastic surface, the maximum error ΔZ_{\max} of the displacement can be expressed as,¹¹

$$\Delta Z_{\max} < \frac{h^3}{4 \cdot R^2} \quad (3)$$

However, the calculated results indicate that the membrane's deflection is much smaller than its diameter, thereby causing the deflection error decreased sharply, which could be neglected in the analysis. Thus, it is reasonable to analyze the elastic surface with a spherical profile in the subsequent study.

Besides, the deformation of the surface is also closely related to the applied pressure P and the membrane's thickness, whose relationship is displayed in the Figure 5(b). With the increasement of the pressure endured on the membrane, the curvature of the surface can be decreased, thereby increasing the lens's focal length.

In order to derive the relationship between the shaft's linear displacement d_m and the lens's focal length f , the elastic surface is simplified as a spherical cap with a radius of curvature R . When the shaft moves d_m in the axial direction, the optical liquid is pushed to redistribute by the driven membrane. The driven membrane displaced volume can be expressed as,

$$V_1 = \frac{1}{2} \cdot \pi \cdot d_m \cdot (r_b^2 + r_p^2) \quad (4)$$

Where r_b and r_p are the radius of the driven membrane and piston respectively.

For the surface deforms in a spherical cap, whose geometrical parameter can be written as,

$$R \approx \frac{r_0^2}{2h} \quad (5)$$

Thus, the volume displayed by the optical membrane is,

$$V_2 = \frac{\pi \cdot h \cdot (3 \cdot \pi^2 \cdot r_0^4 + 4 \cdot h^2)}{24} \quad (6)$$

Where r_0 is the radius of the optical membrane. Since the volume of the stored liquid is constant, so

$$V_1 = V_2 \quad (7)$$

Under this premise, substitute equations (4) and (6) into equation (7), the shaft's linear displacement can be described as,

$$\begin{aligned} d_m &= \frac{h \cdot (3 \cdot \pi^2 \cdot r_0^4 + 4 \cdot h^2)}{12 \cdot (r_b^2 + r_p^2)} \\ &= \frac{6\pi \cdot R \cdot r_0^8 + 32 \cdot R^3}{12 \cdot r_0^6 \cdot (r_b^2 + r_p^2)} \approx \frac{\pi \cdot R \cdot r_0^2}{2 \cdot (r_b^2 + r_p^2)} \end{aligned} \quad (8)$$

It can be seen from the equation that the curvature of the membrane can be changed by improving the motor's linear distance. Moreover, the focal length of

Table 2. Materials used in the piezoelectric motor.

Material	Aluminum alloy	PZT-8H
Density ($\text{kg} \cdot \text{m}^{-3}$)	2810	7650
Poisson's ratio	0.33	0.3
Young's modulus (GPa)	71	$\begin{bmatrix} 120.6 & 53.5 & 51.5 & 0 & 0 & 0 \\ 53.5 & 120.6 & 51.5 & 0 & 0 & 0 \\ 51.5 & 51.5 & 104.5 & 0 & 0 & 0 \\ 0 & 0 & 0 & 31.3 & 0 & 0 \\ 0 & 0 & 0 & 0 & 31.3 & 0 \\ 0 & 0 & 0 & 0 & 0 & 34.6 \end{bmatrix}$
Piezoelectric constant ($\text{C} \cdot \text{m}^{-2}$)	/	$\begin{bmatrix} 0 & 0 & -4.1 \\ 0 & 0 & -4.1 \\ 0 & 0 & 14 \\ 0 & 10.3 & 0 \\ 10.3 & 0 & 0 \\ 0 & 0 & 0 \end{bmatrix}$

the proposed lens can be calculated by the following equation.²⁹

$$f = \frac{R}{n_{\text{liquid}} - 1} \quad (9)$$

Where n_{liquid} represents the refractive index of the optical liquid.

Substitute equation (8) into equation (9), the focal length of the lens can be described as,

$$f = \frac{2 \cdot d_m \cdot (r_b^2 + r_p^2)}{\pi \cdot (n_{\text{liquid}} - 1) \cdot r_0^2} \quad (10)$$

From the equation, the lens's focal length can be adjusted effectively by controlling the motor. Furthermore, the optical power of the lens can be enhanced by choosing an optical liquid of high-index or optimizing the lens's geometrical parameters.

Analysis of the motor

Modal analysis. In order to verify the working principle of the motor and explain its vibration in this chapter, the model analysis of the stator is conducted by the commercial finite element software-ANSYS (Version 18.0).³⁰ The metal elastomer is made up of aluminum alloy, whose Young's modulus is 71 GPa, the Poisson's ratio is 0.33 and the density is $2810 \text{ kg} \cdot \text{m}^{-3}$. Moreover, the material of the piezoelectric elements is PZT-8H, whose piezoelectric constant matrix and elastic stiffness matrix are also demonstrated in Table 2.

In addition, the fine thread in this configuration makes it difficult to complete the modal analysis of the stator. Since the influence of internal threads on the results of modal analysis is so small that can be ignored, the computing model thus is simplified as a

circular cylinder to simulate under the free boundary condition. The vibration modes of the stator by FEM are shown in the Figure 6. The resonant frequency of mode A and B are 12.584 kHz and 12.613 kHz respectively. The frequency difference between two orthogonal modes is 29 Hz, which can substantially meet the design requirement of the motor.

Dynamic response analysis. To validate the dynamic features of the motor, the dynamic response analysis is constructed in a damping coefficient of 0.3%. Based on the modal analysis results, the exciting signals with the peak voltages of 80 V under the frequency of 12.584 kHz, are applied on the piezoelectric elements as illustrated before. Particles *M* and *W* are the points distributed on the stator's surface, whose position is shown in the Figure 7(a). In plane *XOY*, the motion trajectories of the selected points are accomplished by ANSYS plotted in the Figure 7(b). It can be found that these two points move along the same elliptical trajectory, as the travelling wave propagates. However, their phase difference is always π in the exact same moment. That is, these two points move along the ellipse tracking in a counterclockwise direction, but their location is symmetric about the origin of the ellipse.

Experimental investigation

Fabrication

In order to validate the feasibility and practicability of the proposed lens, the prototype with weight of 36.4 g was manufactured by SCNUAA (Nuaa Super Control Technology Co., Ltd, China), as shown in the Figure 8. The material of the lens frame is the aluminum alloy, whose inner and outer diameter is 28 mm and 35 mm respectively. The height of the rim is 2.8 mm and it has a gap of 1 mm in one side.

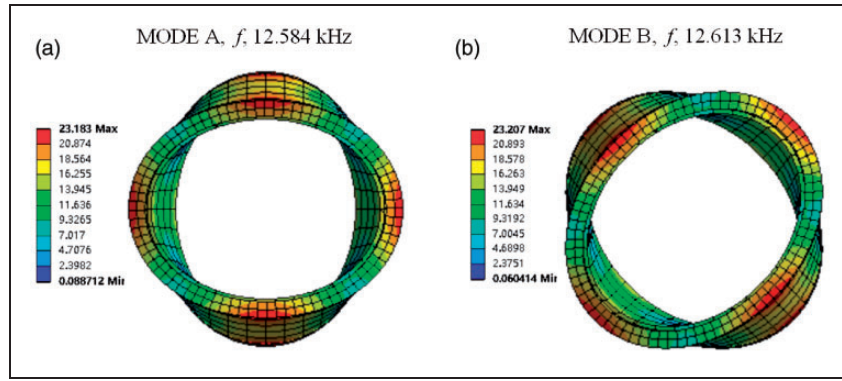


Figure 6. Operating modes of the stator in the simulation: (a) Mode A. (b) Mode B.

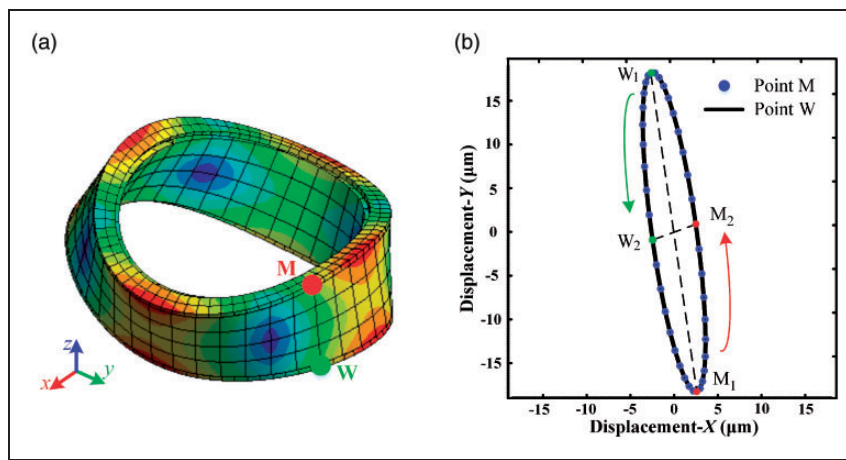


Figure 7. Movement trajectories of the driving surface: (a) Selected points on the stator's surface. (b) Elliptical trajectory of the selected points in plane XOY by FEM.

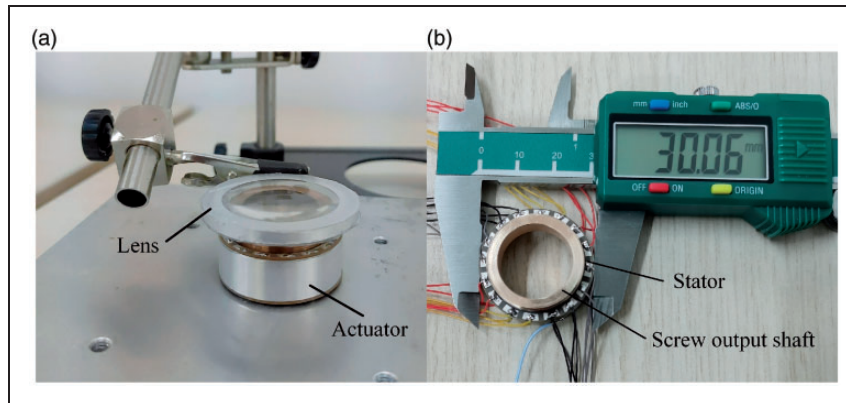


Figure 8. Prototype of the lens: (a) Lens including the actuator. (b) Prototype of the proposed motor.

Besides, the flexible membranes in the lens are made of PDMS, which uses the mixing ratio of 10:1 to fabricate the membrane at 60 °C. The thicknesses of the optical and driven membranes are 0.2 mm and 0.5 mm respectively. And the liquid chamber is sealed by these two parts, which is used to fill the transparent liquid of high index. In this study, glycerol ($n = 1.41$)

with density of $1.26 \text{ g} \cdot \text{cm}^{-3}$ is adopted in the lens. Theoretically, for the incompressibility of glycerol, the liquid can be redistributed in the chamber under the function of the motor. To achieve the automatic zoom of the lens, a piston made of acrylic sheet is placed under the driven membrane. When the output shaft of the motor moves along Z-axis, it

provides a vertical deflection without compromising force for the piston. Furthermore, the stator of the piezoelectric motor is made of aluminum alloy, whose inner and external diameter is 25 mm and 30 mm respectively. The material of the shaft is phosphor bronze, whose external threads can be engaged with the stator's inner threads.

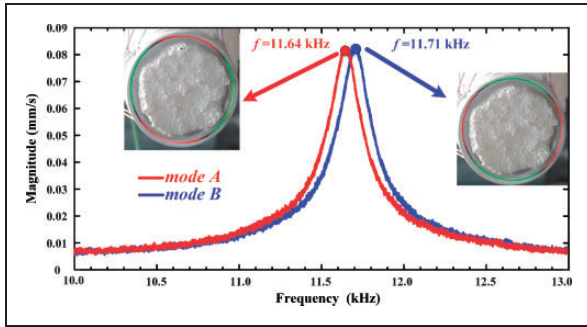


Figure 9. Vibration scanning results of the motor prototype.

Vibration measurement of the motor

The vibration measurement of the proposed motor is accomplished by the Doppler three-dimensional laser scanner (PSV-500-3D, Polytec GmbH, Waldbronn, Germany). In this experiment, the external surface of the stator is selected as the scanning plane. Figure 9 shows the vibration velocity response spectrum and the mode of vibration at the resonant frequency, which keeps consistent with the ideal shape of the mode. The resonant frequency of mode A and B is 11.64 kHz and 11.71 kHz respectively, which is slightly lower than that of the modal simulation.

System performances

To investigate the optical performances of the proposed lens, an experimental test platform was established as displayed in the Figure 10. The platform is composed of a function generator (AFG 3022B,

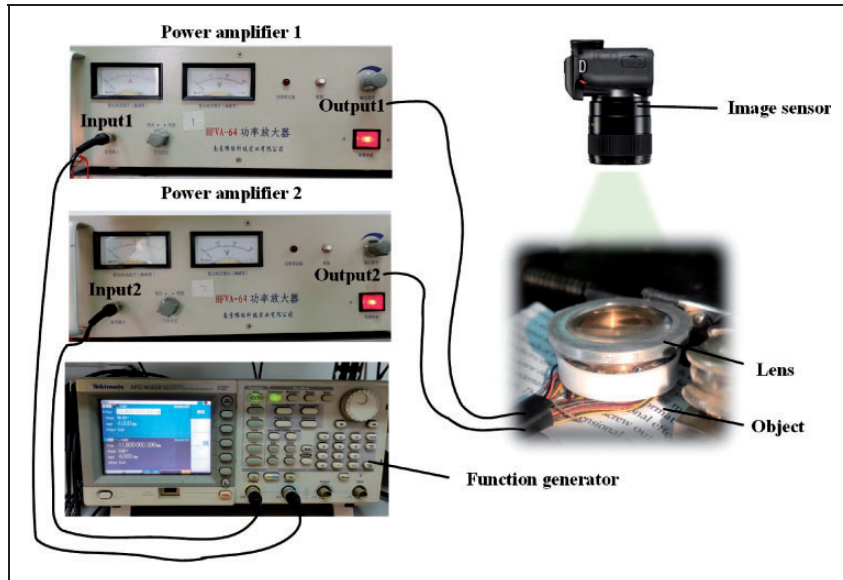


Figure 10. Experimental setup for the lens measurement.

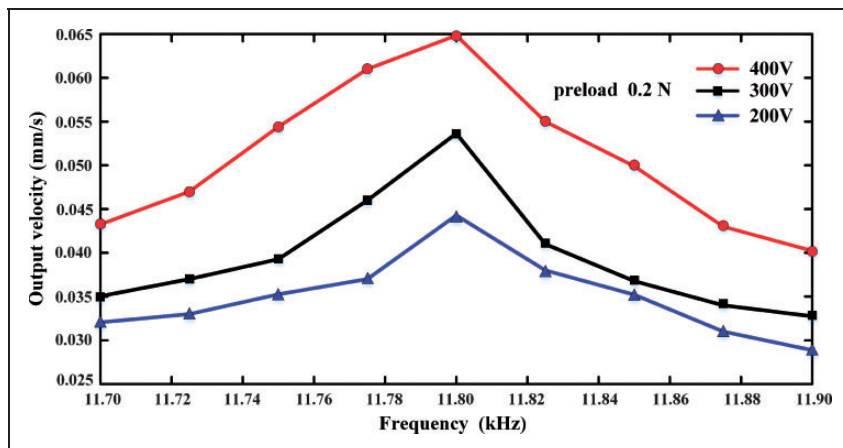


Figure 11. Frequency characteristics of the proposed motor.

Tektronix Inc., USA), two power amplifiers (HFVA-153, Foneng Technology Co., Ltd, China), an object and an image sensor. Specially, the image sensor is a single lens reflex camera with 40 mm focal length, which is used to acquire images at different displacements of the proposed motor. When the test system works, the piezoelectric elements excited by two-phase signals activates the shaft to move along Z-direction, the curvature of the lens surface thus can be changed within a certain range. Due to the output characteristics of the proposed motor are important indicators for evaluating the lens prototype, the motor's performances are tested firstly by the experimental setup.

Figure 11 shows the frequency characteristics of the proposed piezoelectric motor under a preload of 0.2 N. As described in the image, the motor's linear

velocity can be improved by increasing the driving voltages. The result also indicates that the motor prototype can operate steadily and continuously from 11.70 kHz to 11.90 kHz, and its output velocity can reach its peak at 0.065 mm/s when the voltage and excitation frequency are 400 V_{p-p} and 11.80 kHz respectively. Compared with the simulation results, the operating frequency of the motor has a slight deviation, which might be for the unavoidable errors in assembly. Therefore, the frequency of 11.80 kHz is selected as the working frequency in the subsequent experiments.

Figure 12(a) describes the relationship between the output velocity and driving voltages at the preload of 0.2 N, 0.5 N, 0.7 N and 1 N. The result suggests the motor's linear velocity decreases with the increasing load especially under the load of 1 N, which is stated more clearly and intuitively in the Figure 12(b). Under the frequency of 11.80 kHz, it can be seen that the maximum output power is 0.0372 mW at 400 V_{p-p} voltages and 0.7 N loads, while the velocity is about 0.053 mm/s. The piezoelectric motor can thus operate steadily at the ultra-low speed in low load. Due to these mechanical properties, the positioning accuracy of the linear motor can reach the micron level. In conclusion, the proposed motor has the advantages of compact structure, convenient processing and high precision, which can meet the requirements of the drive unit for the liquid lens.

Driven by the piezoelectric motor, the lens prototype thus can provide high-precision adjustment within a certain range. Figure 13 exhibits the images at different displacements of the shaft. It can be seen clearly from the image that the lens's surface aberration can indeed be changed by controlling the motor. As the measurement displayed, the focal length of the lens ranging from 9.6 mm to 17.9 mm can be realized under the actuation of the propose motor, whose imaging result is shown in the Figure 13(b).

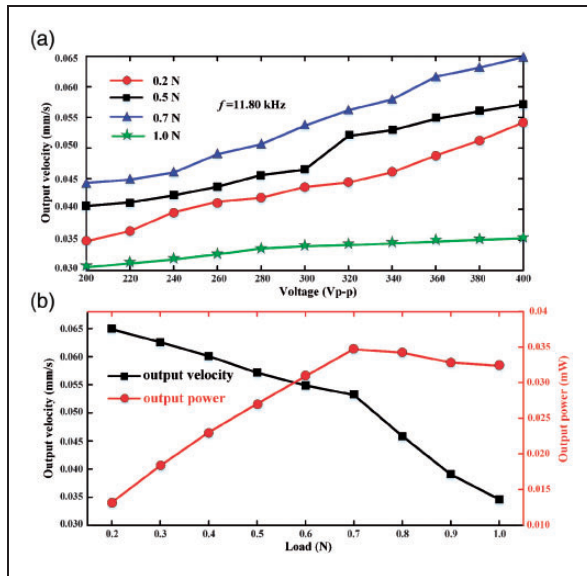


Figure 12. Load characteristics of the proposed motor: (a) Relationship between the output velocity and voltage at different loads. (b) Mechanical characteristics.

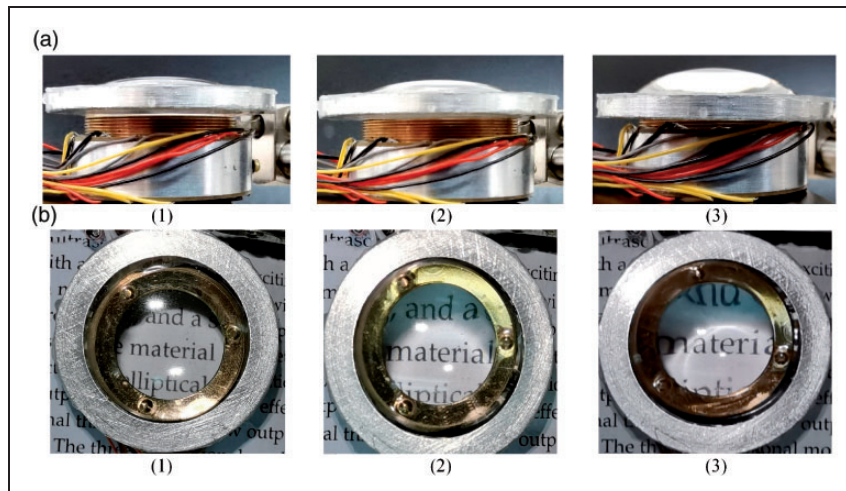


Figure 13. Test images at motor's different displacements of 1 mm, 3 mm and 5 mm: (a) Surface aberration. (b) Imaging result.

Conclusions

In conclusion, a tunable-focus lens actuated by a novel piezoelectric motor is proposed, assembled and investigated in this study. Compared with other adaptive lens, the proposed lens driven by the piezoelectric motor has the advantages of compact structure, easy fabrication process and high-precision. According to the specific application, the lens with aperture diameter of 30 mm is adopted to design and fabricate. The operating principle of the proposed lens is stated in detail. Using the finite element method, the shapes of lens surface under different driving displacements are simulated in the software of ANSYS 18.0, which provides a solid basis for designing the lens. In this configuration, a novel linear piezoelectric motor is used as an actuator to control the extrusion of the lens under different conditions, which provides an external force for the lens. The corresponding experiments are carried out to the investigate the mechanical performances of the lens. And the testing results show the proposed lens can zoom within a range of 8.3 mm by actuating the piezoelectric motor. Although the presented device exhibits well zooming characteristic and stability in the experiment, it is difficult to implement in practice for the system lacks the research on close-loop control scheme and it is expected to be developed gradually in the future research.




Declaration of Conflicting Interests

The author(s) declared no potential conflicts of interest with respect to the research, authorship, and/or publication of this article.

Funding

The author(s) disclosed receipt of the following financial support for the research, authorship, and/or publication of this article: This work was supported by the Foundation of Graduate Innovation Center in NUAA (grant No.kfjj20190105) and the Priority Academic Program Development of Jiangsu Higher Education Institutions (PAPD).

ORCID iDs

Hanlu Li  <https://orcid.org/0000-0002-3898-1188>
 Weihao Ren  <https://orcid.org/0000-0002-6740-5294>
 Lin Yang  <https://orcid.org/0000-0002-6009-8404>

References

1. Khanna R C , Cicinelli M V , Gothwal V K , et al. Innovative Approaches in the Delivery of Eye Care: Children[M]// Innovative Approaches in the Delivery of Primary and Secondary Eye Care. 2019.
2. O'Donoghue L, McClelland JF, Logan NS, et al. Refractive error and visual impairment in school children in Northern Ireland. *Br J Ophthalmol* 2010; 94: 1155–1159.

3. Hiago C. "INFORMATION ON VISUAL IMPAIRMENT ACROSS COUNTRIES." Frenxiv. January 10, 2020. DOI: 10.31226/osf.io/2hqbu.
4. Glasser A and Campbell MC. Presbyopia and the optical changes in the human crystalline lens with age. *Vision Res* 1998; 38: 209–230.
5. Ciuffreda KJ, Rosenfield M, Mordi J, et al. Accommodation, age and presbyopia[M]. In: *Accommodation and vergence mechanisms in the visual system*. Birkhäuser: Basel, 2000, pp.193–200.
6. Furtado JM, Berezovsky A, Ferraz NN, et al. Prevalence and causes of visual impairment and blindness in adults aged 45 years and older from parintins: the Brazilian amazon region eye survey. *Ophthalmol Epidemiol* 2019; 26: 345–354.
7. Naidoo KS and Jaggernath J. Uncorrected refractive errors. *Indian J Ophthalmol* 2012; 60: 432–437.
8. Gills JP and Fenzl RE. Minus-power intraocular lenses to correct refractive errors in myopic pseudophakia. *J Cataract Refract Surg* 1999; 25: 1205–1208.
9. Lord SR, Dayhew J, Sc BA, et al. Multifocal glasses impair edge-contrast sensitivity and depth perception and increase the risk of falls in older people. *J Am Geriatr Soc* 2002; 50: 1760–1766.
10. Callina T and Reynolds TP. Traditional methods for the treatment of presbyopia: spectacles, contact lenses, bifocal contact lenses. *Ophthalmol Clin N Am* 19: 25–33.
11. Ren H, Fox D, Anderson PA, et al. Tunable-focus liquid lens controlled using a servo motor. *Opt Exp* 2006; 14: 8031–8036.
12. Schuhlarden S, Petsch S, Liebetraut P, et al. Miniaturized tunable imaging system inspired by the human eye. *Optics Lett* 2013; 38: 3991–3994.
13. Hasan N, Banerjee A, Kim H, et al. Tunable-focus lens for adaptive eyeglasses. *Opt Exp* 2017; 25: 1221–1233.
14. Liebetraut P, Petsch S, Liebeskind J, et al. Elastomeric lenses with tunable astigmatism. *Light: Sci Appl* 2013; 2: e98–e98.
15. Jeong K-H, Liu GL, Chronis N, et al. Tunable micro-doublet lens array. *Opt Express* 2004; 12: 2494–2500.
16. Oku H, Hashimoto K and Ishikawa M. Variable-focus lens with 1-kHz bandwidth. *Opt Express* 2004; 12: 2138–2149.
17. Nicolas S, Allain M, Bridoux C, et al. Fabrication and characterization of a new varifocal liquid lens with embedded PZT actuators for high optical performances[J]. In: *2015 28th IEEE International Conference on Micro Electro Mechanical Systems (MEMS)*, Estoril, 2015, pp. 65–68.
18. Brusa E and Munteanu MG. Validation of compact models of microcantilever actuators for RF-MEMS design. *Analog Integr Circuits Signal Process* 2009; 59: 191–199.
19. Ballestra A, Brusa E, Munteanu MG, et al. Experimental characterization of electrostatically actuated in-plane bending of microcantilevers. *Microsyst Technol* 2008; 14: 909–918.
20. Benasciutti D, Moro L, Zelenika SA, et al. Vibration energy scavenging via piezoelectric bimorphs of optimized shapes. *Microsyst Technol* 2010; 16: 657–668.
21. Jia SH, Tang ZH, Dong J, et al. *Recent advances in flexible variable-focus lens*. *Chinese Optics* 2015; 8: 535–547.

22. Imabayashi H, Fujimura T and Funakubo T. U.S. Patent No. 5,357,164. Washington, DC: U.S. Patent and Trademark Office, 1994.
23. Zhao C. *Ultrasonic motors: technologies and applications*. Berlin: Springer Science & Business Media, 2011.
24. Zhou T, Chen Y, Lu C, et al. The Development, Application and Expectation of Ultrasonic Motor in Lens Focus[J]. *Small & Special Electrical Machines*, 2007 (11): 18.
25. Zhao C. Operating Mechanism and Modeling of Traveling Wave Rotary Ultrasonic Motor. In: *Ultrasonic Motors*. Springer, Berlin, Heidelberg, 2011. https://doi.org/10.1007/978-3-642-15305-1_5.
26. Zhao C. Operating mechanism and modeling of traveling wave rotary ultrasonic motor. In: *Ultrasonic motors*. Berlin: Springer, 2011, pp.118–160.
27. Zhou J, Ellis AV and Voelcker NH. Recent developments in PDMS surface modification for microfluidic devices. *Electrophoresis* 2010; 31: 2–16.
28. Thompson MK and Thompson JM. *ANSYS mechanical APDL for finite element analysis*. Oxford: Butterworth-Heinemann, 2017.
29. Ren H and Wu S-T. Variable-focus liquid lens by changing aperture. *Appl Physics Lett* 2005; 86: 211107.
30. Brusa E, De Bona F, Gugliotta A, et al. Dynamics modeling of microbeams under electrostatic load. In: *Symposium on design, test, integration and packaging of MEMS/MOEMS* 2003. Piscataway: IEEE, 2003, pp.181–186.